Enantiodetection of cyclic three-level chiral molecules in a driven cavity

Yu-Yuan Chen,[1] Jian-Jian Cheng,[1] Chong Ye,[2] and Yong Li[1,3,*]

[1]*Beijing Computational Science Research Center, Beijing 100193, China*

[2]*Beijing Key Laboratory of Nanophotonics and Ultrafine Optoelectronic Systems, School of Physics, Beijing Institute of Technology, Beijing 100081, China*

[3]*Synergetic Innovation Center for Quantum Effects and Applications, Hunan Normal University, Changsha 410081, China*

(Received 12 November 2021; accepted 25 January 2022; published 10 February 2022)

We propose an enantiodetection method of chiral molecules in a cavity with an external drive. The chiral molecules are coupled with a quantized cavity field and two classical light fields to form the cyclic three-level systems. The chirality-dependent cavity-assisted three-photon process in the three-level systems leads to the generation of intracavity photons. Simultaneously, the drive field also results in a chirality-independent process of the generation of intracavity photons. Based on the interference between the intracavity photons generated from these two processes, one can detect the enantiomeric excess of chiral mixture via monitoring the transmission rate of the drive field. It is also shown that our method can work in the single-molecule weak-coupling region and in the absence of additional enantiopure samples. These advantages make it offer promising applications in enantiodetection of chiral molecules.

DOI: 10.1103/PhysRevResearch.4.013100

I. INTRODUCTION

The existence of two molecular structural forms known as enantiomers (left- and right-handed chiral molecules) is one of the most important manifestations of symmetry breaking in nature [1]. Chiral molecules refer to molecules that cannot be superposed on their mirror images via translations and rotations. They play crucial roles in various enantioselective biological activities and chemical reactions [2,3]. Thus, enantiodetection [4–20] of chiral molecules is important and challenging work. Most conventional spectroscopic methods [4–7] for the enantiodetection of chiral molecules are based on the interference between the electric-dipole and the magnetic-dipole (or electric-quadrupole) transitions, and thus the chiral signals are weak since the magnetic-dipole and electric-quadrupole transition moments are usually weak compared with the electric-dipole transition moments.

Recently, cyclic three-level systems [9–42] of chiral molecules involving only electric-dipole transitions have been widely used in the enantiodetection [9–20], enantiospecific state transfer [28–36], and spatial enantioseparation [37–42] of chiral molecules. Particularly, enantiomer-specific microwave spectroscopic methods [10–14] based on cyclic three-level systems have achieved great success in investigations of the enantiodetection of chiral molecules. Due to the inherent properties of the electric-dipole transition moments of enantiomers, the product of three electric-dipole transition moments for cyclic three-level systems changes sign with the enantiomer. Thus, when the molecules in a chiral mixture are coupled with two classical light fields, the total induced light field generated via the three-photon process of three-wave mixing [10–14] is determined by the difference between the numbers of left- and right-handed molecules. Consequently, one can detect the enantiomeric excess of the chiral mixture via monitoring the intensity of the total induced light field.

On the other hand, cavity quantum electrodynamics (CQED) systems with a single molecule or many molecules confined in a cavity have received considerable interest [43–54]. In such CQED systems, the electromagnetic environment of the molecule(s) is modified by a quantized cavity field. This can strengthen dramatically the interaction between light fields and molecule(s). Thus, the CQED systems have shown promising applications in the fields of energy transfer [44–46], molecular spectra [47–49], and control of chemical reactions [50–52] for molecules.

Most recently, the enantiodetection of single chiral molecule [53] or many chiral molecules [54] has been investigated theoretically in CQED systems. In Ref. [53], it has been proposed to distinguish the chirality of a single chiral molecule by using the single-molecule model of a cyclic three-level system. However, in a realistic case, systems of enantiodetection [4–19] (as well as enantiospecific state transfer [28–36,55,56], spatial enantioseparation [37–42], and enantioconversion [57–65]) of chiral molecules commonly contain a large number of molecules. In the case of quantized cavity field(s) coupling with many molecules, one should resort to the multimolecule treatment [44–52], rather than the single-molecule one, which is only appropriate in the case of classical field(s) interacting with many molecules [4–19]. In Ref. [54], the enantiodetection of a chiral mixture has been

*liyong@csrc.ac.cn

Published by the American Physical Society under the terms of the Creative Commons Attribution 4.0 International license. Further distribution of this work must maintain attribution to the author(s) and the published article's title, journal citation, and DOI.

achieved with a multimolecule treatment in a CQED system for cyclic three-level chiral molecules in a cavity without an external drive. The chirality-dependent cavity-assisted three-photon process leads to the generation of intracavity photons (even in the absence of an external drive to the cavity). Thus it provided a promising way to detect the enantiomeric excess of the chiral mixture by measuring the output field of the cavity.

In this paper, we propose an enantiodetection method based on the CQED system for cyclic three-level chiral molecules, which are located in a traveling-wave cavity [66–68] with an external drive. Each molecule is described by the cyclic three-level system coupled with the quantized cavity field and two classical light fields. In the absence of an external drive, due to the existence of the two classical light fields, intracavity photons can be generated via the chirality-dependent cavity-assisted three-photon process [54]. In the presence of an external drive, the drive field enters the cavity and also results in the chirality-independent process of the generation of intracavity photons. There exists the interference between the intracavity photons resulting from these two processes. Based on this, we demonstrate that enantiomeric excess can be detected by monitoring the steady-state transmission rate of the drive field.

We remark that in the previous system [54] where the cyclic three-level model is designed in a standing-wave cavity, the size of the sample is required to be much smaller than the wavelengths of all the light fields to evade the influence of phase mismatching and the spatial dependence of the coupling strength. In our current system, however, such a strict requirement is not necessary since the present cyclic three-level model is specially designed in the traveling-wave cavity. On the other hand, there is no external drive to the cavity in the previous system [54] and thus additional enantiopure samples are required to further determine the sign of the enantiomeric excess of the chiral mixture in the enantiodetection therein. In contrast, the existence of an external drive to the cavity in our system ensures our present method works without requiring additional enantiopure samples. Therefore, the present method has advantages in the enantiodetection of chiral molecules compared with the previous one in Ref. [54]. In addition, our system involves a collectively enhanced interaction between the quantized cavity field and many molecules, which means our method does not require single-molecule strong coupling to evade the influence of decoherence.

This paper is organized as follows. In Sec. II, we give the model and Hamiltonian of the CQED system for cyclic three-level chiral molecules. Then the steady-state transmission of the drive field is investigated in Sec. III. Further, we present the results for the enantiodetection of chiral molecules in Sec. IV, and then discuss our investigations in Sec. V. Finally, a conclusion is given in Sec. VI.

II. MODEL AND HAMILTONIAN

We consider a CQED system for cyclic three-level chiral molecules as shown in Fig. 1. The system consists of a driven traveling-wave cavity and a chiral mixtures confined in the cavity. The drive field with amplitude ε_d and angular frequency ν_d enters the cavity from mirror $M_{\rm I}$ and exits from mirror $M_{\rm II}$. The chiral mixture contains $N = N_L + N_R$

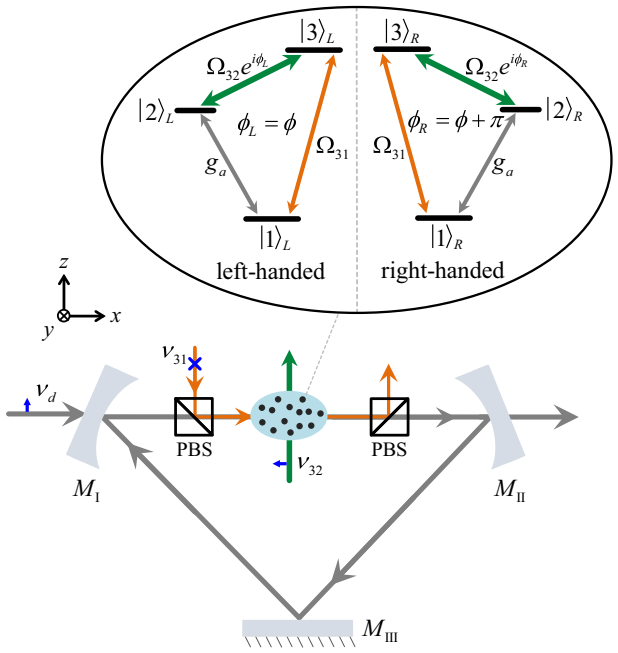

FIG. 1. The model of the CQED system for the cyclic three-level chiral molecules under consideration. The cavity is composed of three mirrors $M_{\rm I}$, $M_{\rm II}$, and $M_{\rm III}$. Here, the mirrors $M_{\rm I}$ and $M_{\rm II}$ are partially reflective and have the same reflection coefficients, while the mirror $M_{\rm III}$ is assumed to be perfectly reflective. The chiral molecules are coupled with the quantized cavity field and two classical light fields to form cyclic three-level systems. The polarization directions of the light fields are shown in blue. The classical light field with angular frequency ν_{31} is introduced through the polarizing beam splitter (PBS) to interact with the molecules.

molecules with N_L and N_R denoting the numbers of left- and right-handed molecules, respectively. The subscript $Q\,(=L,R)$ is introduced to represent the molecular chirality. Each molecule in the chiral mixture is modeled as a cyclic three-level system, where the ground state $|1\rangle_Q$ is coupled to the state $|2\rangle_Q$ by a quantized cavity field with angular frequency ω_a and the state $|1\rangle_Q$ ($|2\rangle_Q$) is coupled to the state $|3\rangle_Q$ by a classical light field with angular frequency ν_{31} (ν_{32}). Here, we focus on the three-photon resonant condition

$$\nu_{31} = \nu_d + \nu_{32}. \tag{1}$$

Under the dipole approximation and rotating-wave approximation, the Hamiltonian in the interaction picture with respect to $H_0 = \nu_d a^\dagger a + \nu_d(S_{22}^L + S_{22}^R) + \nu_{31}(S_{33}^L + S_{33}^R)$ is written in time-independent form as ($\hbar = 1$)

$$\begin{aligned} H_I = {} & \Delta_a a^\dagger a + i\sqrt{\kappa_a}\left(\varepsilon_d a^\dagger - \varepsilon_d^* a\right) \\ & + \Delta_{21}\left(S_{22}^L + S_{22}^R\right) + \Delta_{31}\left(S_{33}^L + S_{33}^R\right) \\ & + \left[g_a a\left(S_{21}^L + S_{21}^R\right) + \Omega_{31}\left(S_{31}^L + S_{31}^R\right)\right. \\ & \left. + \Omega_{32}\left(e^{i\phi_L}S_{32}^L + e^{i\phi_R}S_{32}^R\right) + \text{H.c.}\right], \end{aligned} \tag{2}$$

where $\Delta_a = \omega_a - \nu_d$, $\Delta_{21} = \omega_{21} - \nu_d$, and $\Delta_{31} = \omega_{31} - \nu_{31}$ are the detunings, with ω_{21} and ω_{31} denoting the transition angular frequencies. a ($a^\dagger$) is the annihilation (creation) operator of the quantized cavity field. Here, both the cavity decay rates from mirror $M_{\rm I}$ and mirror $M_{\rm II}$ are assumed to be $\kappa_a/2$, while

other cavity decay rates have been neglected. Thus, the total cavity decay rate is equal to κ_a. For simplicity but without loss of generality, the amplitude of the drive field ε_d is taken as real. $S^Q_{jk} = \sum_{m=1}^{N_Q} |j\rangle^Q_m {}^Q_m\langle k|$ $(j,k=1,2,3)$ are introduced to denote the collective operators for the chiral molecules. g_a represents the coupling strength between the quantized cavity field and single molecules, and Ω_{31} and $\Omega_{32}e^{i\phi_Q}$ denote the coupling strengths between the two classical light fields and single molecules. Here, g_a, Ω_{31}, and Ω_{32} are assumed to be identical for all the molecules and are taken as real. ϕ_L and ϕ_R are the overall phases of the three coupling strengths in cyclic three-level systems of left- and right-handed molecules, and the chirality of the cyclic three-level system is specified as

$$\phi_L = \phi, \quad \phi_R = \phi + \pi. \tag{3}$$

In our CQED system, when the chiral molecules confined in the cavity are coupled with the two classical light fields, the cavity-assisted three-photon process can result in the generation of intracavity photons [54]. Meanwhile, the drive field can also lead to the process of the generation of intracavity photons. The interference between the intracavity photons resulting from these two processes determines the output field of the cavity, which provides a way to detect the enantiomeric excess by monitoring the output field (e.g., the transmission rate of the drive field). Therefore, our method is different from that in Ref. [54], wherein only the intracavity photons generated from the cavity-assisted three-photon process determine the output field of the cavity due to the absence of an external drive.

Furthermore, these collective operators S^Q_{jk} can be expressed by introducing the generalized Holstein-Primakoff transformation [69–75] as

$$S^Q_{11} = N_Q - A^\dagger_Q A_Q - B^\dagger_Q B_Q, \quad S^Q_{22} = A^\dagger_Q A_Q, \quad S^Q_{33} = B^\dagger_Q B_Q,$$
$$S^Q_{21} = A^\dagger_Q \sqrt{S^Q_{11}}, \quad S^Q_{31} = B^\dagger_Q \sqrt{S^Q_{11}}, \quad S^Q_{32} = B^\dagger_Q A_Q, \tag{4}$$

where A_Q $(A^\dagger_Q)$ and B_Q $(B^\dagger_Q)$ obey the standard bosonic commutation relations $[A_Q, A^\dagger_Q] = [B_Q, B^\dagger_Q] = 1$ and $[A_Q, B_Q] = [A_Q, B^\dagger_Q] = 0$. In the low-excitation limit of molecules with large N_Q limit (i.e., most molecules stay at their ground states: $\langle A^\dagger_Q A_Q + B^\dagger_Q B_Q\rangle \ll N_Q$) [22,73–75], the operator $A^\dagger_Q$ $(B^\dagger_Q)$ here represents the collective excitation from the ground state $|1\rangle_Q$ to the excited state $|2\rangle_Q$ $(|3\rangle_Q)$. Moreover, $A^\dagger_Q A_Q$ $(B^\dagger_Q B_Q)$ denotes the population for the excited state $|2\rangle_Q$ $(|3\rangle_Q)$. Therefore, in the low-excitation limit of molecules with a large N_Q limit, Hamiltonian (2) is rewritten as

$$\begin{aligned} H_I \simeq\ & \Delta_a a^\dagger a + i\sqrt{\kappa_a}\varepsilon_d(a^\dagger - a) \\ & + \Delta_{21}(A^\dagger_L A_L + A^\dagger_R A_R) + \Delta_{31}(B^\dagger_L B_L + B^\dagger_R B_R) \\ & + \big[g_a a(\sqrt{N_L}A^\dagger_L + \sqrt{N_R}A^\dagger_R) + \Omega_{31}(\sqrt{N_L}B^\dagger_L + \sqrt{N_R}B^\dagger_R) \\ & + \Omega_{32}(B^\dagger_L A_L e^{i\phi_L} + B^\dagger_R A_R e^{i\phi_R}) + \text{H.c.}\big]. \end{aligned} \tag{5}$$

In the following discussions, we will use 1,2-propanediol as an example to demonstrate our method. The working states of the cyclic three-level system are chosen as $|1\rangle = |g\rangle|0_{000}\rangle$, $|2\rangle = |e\rangle|1_{110}\rangle$, and $|3\rangle = (|e\rangle|1_{101}\rangle + |e\rangle|1_{10-1}\rangle)/\sqrt{2}$, with $|g\rangle$ $(|e\rangle)$ denoting the vibrational ground (first-excited) state for the motion of OH stretch with the transition angular frequency $\omega_{\text{vib}} = 2\pi \times 100.950$ THz [76]. The rotational states are marked in the $|J_{K_a K_c M}\rangle$ notation [34,77]. Correspondingly, as shown in Fig. 1, the state $|1\rangle$ is coupled to the state $|2\rangle$ by the z-polarized quantized field in the cavity, which is driven by the z-polarized classical light field. The state $|1\rangle$ $(|2\rangle)$ is coupled to the state $|3\rangle$ by the y-polarized (x-polarized) classical light field. According to the rotational constants for 1,2-propanediol, $A = 2\pi \times 8524.405$ MHz, $B = 2\pi \times 3635.492$ MHz, and $C = 2\pi \times 2788.699$ MHz [78], the bare transition angular frequencies are obtained as $\omega_{21} = 2\pi \times 100.961$ THz, $\omega_{31} = 2\pi \times 100.962$ THz, and $\omega_{32} = 2\pi \times 0.847$ GHz [77]. We would like to remark that our model and method are applicable for general (asymmetric-top) gaseous chiral molecules, though we take 1,2-propanediol as an example in the discussions.

III. STEADY-STATE TRANSMISSION

In this section, we study the transmission of the drive field in the steady state and explore its potential applications in the enantiodetection of a chiral mixture.

According to Hamiltonian (5), one can obtain the quantum Langevin equations for the system as

$$\begin{aligned} \dot{a} =& -K_a a - ig_a(\sqrt{N_L}A_L + \sqrt{N_R}A_R) + \sqrt{\kappa_a}(\varepsilon_d + a^{\text{I}}_{\text{in}} + a^{\text{II}}_{\text{in}}), \\ \dot{A}_Q =& -K_A A_Q - ig_a\sqrt{N_Q}a - i\Omega_{32}e^{-i\phi_Q}B_Q + F^Q_A, \\ \dot{B}_Q =& -K_B B_Q - i\Omega_{31}\sqrt{N_Q} - i\Omega_{32}e^{i\phi_Q}A_Q + F^Q_B, \end{aligned} \tag{6}$$

where $K_a = i\Delta_a + \kappa_a$, $K_A = i\Delta_{21} + \Gamma_A$, and $K_B = i\Delta_{31} + \Gamma_B$. a^{I}_{in} $(a^{\text{II}}_{\text{in}})$ is the quantum input noise operator from mirror M_{I} (M_{II}) of the cavity, and has a zero-mean value (i.e., $\langle a^{\text{I}}_{\text{in}}\rangle = \langle a^{\text{II}}_{\text{in}}\rangle = 0$). Γ_A (Γ_B) is introduced to denote the decay rate of the collective mode A_Q (B_Q). F^Q_A (F^Q_B) is the quantum input noise term of the collective operator A_Q (B_Q), and has a zero-mean value (i.e., $\langle F^Q_A\rangle = \langle F^Q_B\rangle = 0$). Therefore, we obtain the following steady-state equations,

$$\begin{aligned} 0 =& -K_a\langle a\rangle - ig_a(\sqrt{N_L}\langle A_L\rangle + \sqrt{N_R}\langle A_R\rangle) + \sqrt{\kappa_a}\varepsilon_d, \\ 0 =& -K_A\langle A_Q\rangle - ig\sqrt{N_Q}\langle a\rangle - i\Omega_{32}e^{-i\phi_Q}\langle B_Q\rangle, \\ 0 =& -K_B\langle B_Q\rangle - i\Omega_{31}\sqrt{N_Q} - i\Omega_{32}e^{i\phi_Q}\langle A_Q\rangle, \end{aligned} \tag{7}$$

where $\langle O\rangle$ (with $O = a$, A_Q, B_Q) represents the mean value of the operator O. Thus, the steady-state value of $\langle a\rangle$ is given by

$$\langle a\rangle = \frac{i(N_L - N_R)g_a\Omega_{31}\Omega_{32}e^{-i\phi} + \sqrt{\kappa_a}\varepsilon_d(K_A K_B + \Omega^2_{32})}{K_a(K_A K_B + \Omega^2_{32}) + g^2_a N K_B}. \tag{8}$$

From Eq. (8), one can understand the physical mechanism underlying our method as follows. In the absence of an external drive (i.e., $\varepsilon_d = 0$), only the first term in the numerator, which results from the chirality-dependent cavity-assisted three-photon process for the chiral mixture [54], contributes to the intracavity photons. This term is proportional to $N_L - N_R$ since $g_a\Omega_{31}\Omega_{32}e^{-i\phi_Q}$ changes sign with the enantiomer. When an external drive is applied (i.e., $\varepsilon_d \neq 0$), the second term in

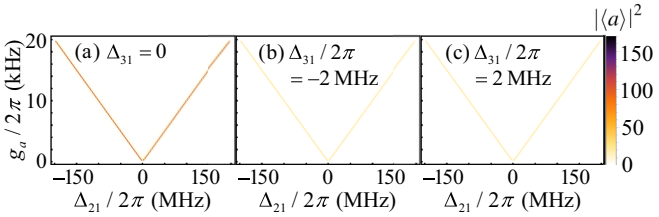

FIG. 2. The steady-state intracavity mean photon number $|\langle a\rangle|^2$ in the absence of an external drive ($\varepsilon_d = 0$) vs the detuning Δ_{21} and the coupling strength g_a for (a) $\Delta_{31} = 0$, (b) $\Delta_{31}/2\pi = -2$ MHz, and (c) $\Delta_{31}/2\pi = 2$ MHz when taking $\eta = 0.9$. The other parameters are chosen as $\Delta_a = \Delta_{21}$, $N = 10^8$, $\Gamma_A/2\pi = \Gamma_B/2\pi = 0.1$ MHz, $\kappa_a/2\pi = 1$ MHz, $\Omega_{31}/2\pi = 8$ kHz, $\Omega_{32}/2\pi = 20$ kHz, and $\phi = 0$.

the numerator of Eq. (8) appears, resulting from the chirality-independent generation process of intracavity photons due to the drive field. Consequently, the interference between the intracavity photons generated from these two processes determines the output field of the cavity, which depends on the enantiomeric excess [17–19] $\eta \equiv (N_L - N_R)/N$.

According to the input-output relation at mirrors $M_{\rm I}$ and $M_{\rm II}$ of the cavity [79–81]

$$\begin{aligned}\sqrt{\kappa_a}a &= a_{\rm in}^{\rm I} + a_{\rm out}^{\rm I} + \varepsilon_d,\\ \sqrt{\kappa_a}a &= a_{\rm in}^{\rm II} + a_{\rm out}^{\rm II},\end{aligned} \tag{9}$$

one can obtain the mean output field from mirror $M_{\rm II}$ of the cavity $\langle a_{\rm out}^{\rm II}\rangle = \sqrt{\kappa_a}\langle a\rangle$. Therefore, the steady-state transmission rate of the drive field $T \equiv |\langle a_{\rm out}^{\rm II}\rangle/\varepsilon_d|^2$ is given by

$$T = \frac{\kappa_a}{\varepsilon_d^2}\left|\frac{iNg_a\Omega_{31}\Omega_{32}e^{-i\phi}\eta + \sqrt{\kappa_a}\varepsilon_d(K_AK_B+\Omega_{32}^2)}{g_a^2NK_B + K_a(K_AK_B+\Omega_{32}^2)}\right|^2. \tag{10}$$

In what follows, we further assume that the quantized cavity field is resonantly coupled with the transition $|2\rangle_Q \leftrightarrow |1\rangle_Q$, which means $\Delta_a = \Delta_{21}$, and we assume the total number of chiral molecules $N = 10^8$ [43,51], the decay rates of molecules $\Gamma_A/2\pi = \Gamma_B/2\pi = 0.1$ MHz [10,11], and the total cavity decay rate $\kappa_a/2\pi = 1$ MHz [82,83]. Here, we take the weak coupling strength $\Omega_{31}/2\pi = 8$ kHz since such a weak coupling strength usually ensures the low-excitation limit of molecules.

In the present work, the chirality-dependent cavity-assisted three-photon process is essential in the detection of enantiomeric excess. Thus, we first consider the case in the absence of an external drive (i.e., $\varepsilon_d = 0$) and display the corresponding steady-state intracavity mean photon number $|\langle a\rangle|^2$ versus the detuning Δ_{21} and the coupling strength g_a for different detunings Δ_{31} in Fig. 2. As can be seen from Fig. 2(a), the intracavity mean photon number reaches a maximum $|\langle a\rangle|^2 \simeq 180$ at the detunings $\Delta_{21} \simeq \pm g_a\sqrt{N}$. This is the result of vacuum Rabi splitting induced by a quantized cavity field in the strong collective coupling condition [45,51,81,84]. Here, it is worth mentioning that since the molecules are collectively coupled to the common quantized cavity field in our system, the collective coupling strength (between the quantized cavity field and the collective mode A_Q) $g_a\sqrt{N}$ can be strong even though the single-molecule coupling strength (between the quantized cavity field and single molecules) g_a is weak. Such a collectively enhanced coupling strength releases the technical requirements for strong single-molecule coupling strength, which is usually necessary to evade the influence of decoherence in the enantiodetection methods involving only the classical light fields interacting with molecules [9,17,19]. Moreover, it is found that there are more intracavity photons in the resonant case $\Delta_{31} = 0$ compared with the nonresonant case $\Delta_{31} \neq 0$ [see Figs. 2(a)–2(c)]. In the further discussions, we take the coupling strength $g_a/2\pi = 10$ kHz and the detuning $\Delta_{31} = 0$.

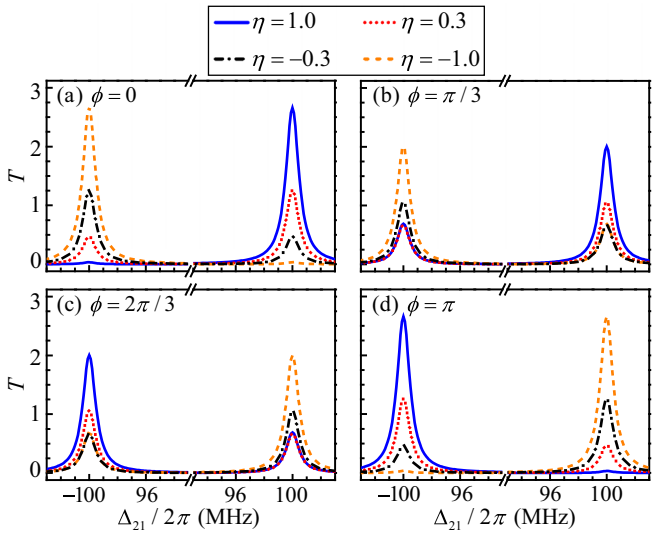

FIG. 3. The transmission rate of the drive field T as a function of the detuning Δ_{21} for different enantiomeric excesses η when the overall phase is taken as (a) $\phi = 0$, (b) $\phi = \pi/3$, (c) $\phi = 2\pi/3$, and (d) $\phi = \pi$. The other parameters are the same as those in Fig. 2 except $\varepsilon_d^2/2\pi = 400$ MHz, $g_a/2\pi = 10$ kHz, and $\Delta_{31} = 0$.

Furthermore, we consider the case in the presence of an external drive (i.e., $\varepsilon_d \neq 0$). In order to investigate the influence of the overall phase ϕ on the transmission rate of the drive field T, we choose different ϕ to give T versus the detuning Δ_{21} in Fig. 3. Here, only the results within the region $\phi \in [0,\ \pi]$ (e.g., $\phi = 0$, $\phi = \pi/3$, $\phi = 2\pi/3$, and $\phi = \pi$) are displayed since the results corresponding to left- and right-handed molecules will exchange when replacing the overall phase ϕ in the region $\phi \in [0,\ \pi]$ by $\phi + \pi$. Here, we find the transmission rate can be larger than one (i.e., $T > 1$). This is the result of the constructive interference between the intracavity photons resulting from the cavity-assisted three-photon process and those generated from the drive field. Moreover, it is also shown that the transmission rate of the drive field is dependent on the overall phase. The underlying physics is that the interference between the intracavity photons generated from the cavity-assisted three-photon process and those resulting from the drive field strongly depends on the overall phase ϕ [see Eq. (8)]. Specifically, for the overall phase $\phi = n\pi$ (with n an arbitrary integer) [see Figs. 3(a) and 3(d)], T becomes relatively sensitive to η compared with the case of other values of ϕ.

IV. DETECTION OF ENANTIOMERIC EXCESS

In this work, we focus on detecting the enantiomeric excess η via measuring the transmission rate of the drive field T. On one hand, we expect that a given T corresponds to only a unique η. That means η can be detected via monitoring T without requiring additional enantiopure samples to further determine the sign of the enantiomeric excess. On the other hand, we expect to achieve a high resolution of detection, which requires that T varies significantly with η.

In the following simulations of this section, the detuning Δ_a, the total number of chiral molecules N, the decay rates of molecules (Γ_A and Γ_B), and the coupling strength Ω_{31} are taken as the same values as those in Sec. III. Moreover, we assume the coupling strength $g_a/2\pi = 10$ kHz and the detuning $\Delta_{31} = 0$.

As discussed above (see Fig. 3), at the detunings $\Delta_{21} \simeq \pm g_a\sqrt{N}$, the transmission rate of the drive field for $\phi = n\pi$ is relatively sensitive to the enantiomeric excess compared with the case of other values of Δ_{21}. Therefore, for simplicity, we here focus on the optimal transmission rate at $\Delta_{21} = g_a\sqrt{N}$,

$$T_{\rm op} \simeq \frac{\kappa_a}{\varepsilon_d^2}\left(\frac{\sqrt{\kappa_a}\varepsilon_d\Gamma_B \pm \sqrt{N}\Omega_{31}\Omega_{32}\eta}{\Gamma_A\Gamma_B + \kappa_a\Gamma_B + \Omega_{32}^2}\right)^2, \tag{11}$$

which is obtained by substituting $\Delta_{21} = g_a\sqrt{N}$ into Eq. (10) and considering the approximation $g_a\sqrt{N} \gg \{\kappa_a, \Gamma_A, \Gamma_B, \Omega_{32}, \Omega_{31}\}$. In the numerator of Eq. (11), "+" and "−" correspond respectively to the case of $\phi = 2n\pi$ and $\phi = (2n+1)\pi$. It is found from Eq. (11) that, when the parameters satisfy the condition

$$\sqrt{\kappa_a}\varepsilon_d\Gamma_B \geqslant \sqrt{N}\Omega_{31}\Omega_{32}, \tag{12}$$

$T_{\rm op}$ varies with η monotonically. That means a given transmission rate corresponds to only a unique enantiomeric excess. Thus, here the additional enantiopure samples are not required in the enantiodetection.

According to Eqs. (11) and (12), we further introduce the difference between the optimal transmission rates for purely left-handed ($\eta = 1$) and purely right-handed ($\eta = -1$) chiral mixtures

$$\Delta T_{\rm op} = T_{\rm op}|_{\eta=1} - T_{\rm op}|_{\eta=-1} \tag{13}$$

to evaluate the resolution of detection, where $T_{\rm op}|_{\eta=1}$ ($T_{\rm op}|_{\eta=-1}$) is obtained by substituting $\eta = 1$ ($\eta = -1$) into Eq. (11). In Fig. 4(a), we display $\Delta T_{\rm op}$ versus the coupling strength Ω_{32} and the intensity of the drive field ε_d^2. Here, we take the overall phase $\phi = 0$. It is shown that $\Delta T_{\rm op}$ strongly depends on Ω_{32} and ε_d^2. Particularly, for the total cavity decay rate $\kappa_a/2\pi = 1$ MHz, one finds $\Delta T_{\rm op} \simeq 3$ when taking $\Omega_{32}/2\pi \simeq 25$ kHz and $\varepsilon_d^2/2\pi \simeq 400$ MHz [see point A in Fig. 4(a)]. For the larger total cavity decay rate $\kappa_a/2\pi = 4$ MHz, one obtains $\Delta T_{\rm op} \simeq 3.8$ when taking $\Omega_{32}/2\pi \simeq 50$ kHz and $\varepsilon_d^2/2\pi \simeq 400$ MHz [see point B in Fig. 4(b)].

Based on the results in Fig. 4, we further take $\kappa_a/2\pi = 4$ MHz, $\Omega_{32}/2\pi = 50$ kHz, and $\varepsilon_d^2/2\pi = 400$ MHz to display the optimal transmission rate $T_{\rm op}$ as a function of the enantiomeric excess η for different overall phases. It is found in Fig. 5(a) that, for $\phi = 0$ ($\phi = \pi$), $T_{\rm op}$ is relatively sensitive to η in the region $\eta \in (0, 1)$ [$\eta \in (-1, 0)$] compared with the case in the region $\eta \in (-1, 0)$ [$\eta \in (0, 1)$]. Therefore, to ensure that the enantiomeric excess can be detected accurately via monitoring the transmission rate, the overall phase should be adjusted as $\phi = 0$ ($\phi = \pi$) when the left-handed (right-handed) molecules are dominant in the chiral mixture.

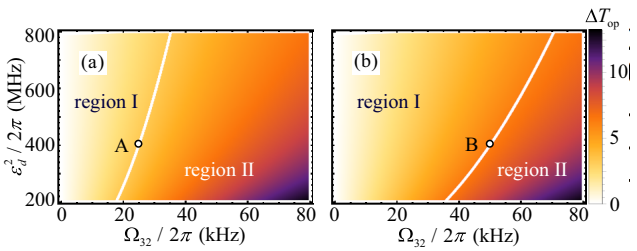

FIG. 4. $\Delta T_{\rm op}$ in Eq. (13) vs the coupling strength Ω_{32} and the intensity of the drive field ε_d^2 when the total cavity decay rate is taken as (a) $\kappa_a/2\pi = 1$ MHz and (b) $\kappa_a/2\pi = 4$ MHz. In region I where the condition $\sqrt{\kappa_a}\varepsilon_d\Gamma_B \geqslant \sqrt{N}\Omega_{31}\Omega_{32}$ is satisfied, $T_{\rm op}$ varies with η monotonically. In region II where the condition $\sqrt{\kappa_a}\varepsilon_d\Gamma_B < \sqrt{N}\Omega_{31}\Omega_{32}$ is satisfied, $T_{\rm op}$ varies with η nonmonotonically. The other parameters are chosen as $\Delta_a = \Delta_{21}$, $N = 10^8$, $\Gamma_A/2\pi = \Gamma_B/2\pi = 0.1$ MHz, $\Omega_{31}/2\pi = 8$ kHz, $g_a/2\pi = 10$ kHz, $\Delta_{31} = 0$, $\Delta_{21}/2\pi = 100$ MHz, and $\phi = 0$.

V. DISCUSSIONS

Here, it is worth mentioning that the above results are based on the low-excitation limit of molecules with a large N_Q limit (i.e., $\langle A_Q^\dagger A_Q + B_Q^\dagger B_Q\rangle \ll N_Q$). Thus, we introduce the factor

$$P_e = \frac{\langle A_L^\dagger A_L + B_L^\dagger B_L\rangle}{N_L} + \frac{\langle A_R^\dagger A_R + B_R^\dagger B_R\rangle}{N_R} \tag{14}$$

to verify whether or not the parameters used for simulations meet such a limit. The first (second) term in Eq. (14) denotes the proportion of left- (right-) handed molecules occupying their excited states to the total ones N_L (N_R). Here, we take the mean-field approximation [81] $\langle A_Q^\dagger A_Q\rangle \simeq \langle A_Q^\dagger\rangle\langle A_Q\rangle$ and $\langle B_Q^\dagger B_Q\rangle \simeq \langle B_Q^\dagger\rangle\langle B_Q\rangle$. The steady-state solutions $\langle A_Q\rangle$, $\langle A_Q^\dagger\rangle$, $\langle B_Q\rangle$, and $\langle B_Q^\dagger\rangle$ are obtained by solving the steady-state Eq. (7). For the parameters in Fig. 5(a), we find $P_e \simeq 1.28 \times 10^{-2}$ [see Fig. 5(b)]. This implies that most molecules stay at

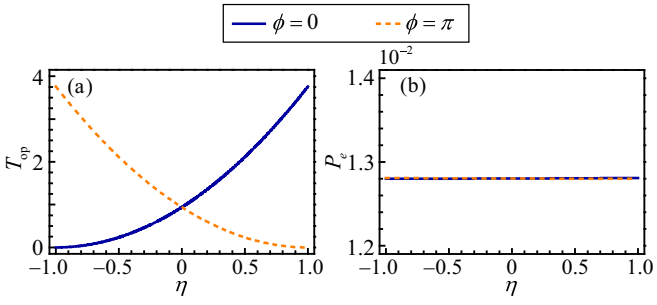

FIG. 5. (a) The optimal transmission rate $T_{\rm op}$ and (b) the factor P_e vs the enantiomeric excess η for different overall phases. The other parameters are the same as those in Fig. 4 except $\kappa_a/2\pi = 4$ MHz, $\Omega_{32}/2\pi = 50$ kHz, and $\varepsilon_d^2/2\pi = 400$ MHz.

their ground states, and thus the results meet the requirement for the low-excitation limit of molecules.

Note that in the previous CQED system for cyclic three-level chiral molecules in a standing-wave cavity [54], the finite size of the sample usually would lead to the phase-mismatching problem [16] and a space-dependent coupling strength [80] between the quantized cavity field and single molecules. In order to evade the influence of the phase mismatching and the spatial dependence of the coupling strength, the size of sample l should be much smaller than all the wavelengths of the classical light fields and the quantized cavity field, that is, $\{|\vec{k}_a|, |\vec{k}_{32}|, |\vec{k}_{31}|\}l \ll 2\pi$. In the present method, we use the system for three-level chiral molecules confined in the traveling-wave cavity [66–68]. When the spatial distribution of molecules is considered, only g_a should be replaced by $g_a e^{i\Delta\vec{k}\cdot\vec{r}_m}$ (with the coupling strengths Ω_{31} and Ω_{32} remaining unchanged) to investigate the influence of the phase mismatching with $\Delta\vec{k} = \vec{k}_{31} - \vec{k}_a - \vec{k}_{32}$, where $\vec{r}_m$ is the position of the mth molecule. To ensure that the influence of the phase mismatching is negligible, the size of sample l should meet the requirement $|\Delta\vec{k}|l \ll 2\pi$. In the present system, $\vec{k}_{32}$ is the smallest one among the three vectors. Thus, by taking $\vec{k}_{31}$ and $\vec{k}_a$ to be parallel and $\vec{k}_{32}$ to be perpendicular to them (see Fig. 1), one can minimize the effect of the phase mismatching. Here, we obtain $|\Delta\vec{k}| \simeq 2\pi \times 4.235\ \mathrm{m}^{-1}$ for the present model of 1,2-propanediol. That means when the sample is fixed in a volume with its size $l \ll 2\pi/|\Delta\vec{k}| \simeq 0.236$ m, the influence of the phase mismatching can be neglected reasonably. Therefore, the requirement (i.e., the size of the sample should be much smaller than the wavelengths of all the light fields) in the previous CQED method [54] is released in our current method since the related cyclic three-level model is specially designed in the traveling-wave cavity.

VI. CONCLUSION

In conclusion, we have proposed an enantiodetection method based on the CQED system for cyclic three-level chiral molecules. The key idea is to achieve the interference between the intracavity photons generated via the cavity-assisted three-photon process and those arising from the drive field. Our results show that the enantiomeric excess can be detected via measuring the steady-state transmission rate of the drive field. In the previous CQED method [54] and enantiomer-specific microwave spectroscopic methods [10–14] for the enantiodetection of chiral molecules, usually the additional enantiopure samples are required to further determine the sign of the enantiomeric excess. Note that the preparation of enantiopure samples remains a challenging work for many chiral molecules [28–42,55–65]. In our method, however, such additional enantiopure samples are not required since our method is based on the interference between the intracavity photons generated via the chirality-dependent cavity-assisted three-photon process and those arising from the chirality-independent drive field. Therefore, our method provides promising applications in the detection of enantiomeric excess for the chiral molecules whose enantiopure samples are still difficult to prepare.

We would like to emphasize that our enantiodetection method involving merely the electric-dipole transitions is preferable to the conventional spectroscopic ones [4–7] involving the interference between electric-dipole and magnetic-dipole (or electric-quadrupole) transitions, since the magnetic-dipole and electric-quadrupole transition moments are usually much weaker than the electric-dipole ones. In addition, different from the enantiomer-specific microwave spectroscopic methods [10–14] involving only the interaction between classical light fields and single molecules in a cyclic three-level model, our method involves a collectively enhanced interaction between the quantized cavity field and collective molecules. This ensures our method can work in the single-molecule weak-coupling region. Moreover, in our system, the intracavity photons are output from the cavity along the direction of the cavity axis, which provides convenience for the collection of the signal. Therefore, our method offers a powerful way to achieve the enantiodetection of chiral molecules.

Note that besides the enantiodetection of chiral molecules [53,54], the CQED systems had also been used in studying the energy transfer [44–46] and control of chemical reactions [50–52] for molecules due to their potential applications in manipulating the molecular dynamical evolution. Therefore, in future investigations, we will further focus on the ambitious issues related to chiral molecules involving molecular dynamical evolution (such as enantiospecific state transfer, spatial enantioseparation, and enantioconversion of chiral molecules) based on CQED systems for cyclic three-level chiral molecules.

ACKNOWLEDGMENTS

This work was supported by the Natural Science Foundation of China (Grants No. 12074030 and No. U1930402), National Science Foundation for Young Scientists of China (No. 12105011), and Beijing Institute of Technology Research Fund Program for Young Scholars.

[1] R. G. Woolley, Quantum theory and molecular structure, Adv. Phys. **25**, 27 (1976).

[2] A. J. Hutt and S. C. Tan, Drug chirality and its clinical significance, Drugs **52**, 1 (1996).

[3] J. Gal, The discovery of stereoselectivity at biological receptors: Arnaldo Piutti and the taste of the asparagine enantiomers—History and analysis on the 125th anniversary, Chirality **24**, 959 (2012).

[4] L. D. Barron, *Molecular Light Scattering and Optical Activity* (Cambridge University Press, Cambridge, UK, 1982).

[5] P. J. Stephens, Theory of vibrational circular dichroism, J. Phys. Chem. **89**, 748 (1985).

[6] R. K. Kondru, P. Wipf, and D. N. Beratan, Atomic contributions to the optical rotation angle as a quantitative probe of molecular chirality, Science **282**, 2247 (1998).

[7] R. Bielski and M. Tencer, Absolute enantioselective separation: Optical activity ex machina, J. Sep. Sci. **28**, 2325 (2005).

[8] D. Zhai, P. Wang, R.-Y. Wang, X. Tian, Y. Ji, W. Zhao, L. Wang, H. Wei, X. Wu, and X. Zhang, Plasmonic polymers with strong chiroptical response for sensing molecular chirality, Nanoscale **7**, 10690 (2015).

[9] W. Z. Jia and L. F. Wei, Probing molecular chirality by coherent optical absorption spectra, Phys. Rev. A **84**, 053849 (2011).

[10] D. Patterson, M. Schnell, and J. M. Doyle, Enantiomer-specific detection of chiral molecules via microwave spectroscopy, Nature (London) **497**, 475 (2013).

[11] D. Patterson and J. M. Doyle, Sensitive Chiral Analysis via Microwave Three-Wave Mixing, Phys. Rev. Lett. **111**, 023008 (2013).

[12] V. A. Shubert, D. Schmitz, D. Patterson, J. M. Doyle, and M. Schnell, Identifying enantiomers in mixtures of chiral molecules with broadband microwave spectroscopy, Angew. Chem., Int. Ed. **53**, 1152 (2014).

[13] S. Lobsiger, C. Pérez, L. Evangelisti, K. K. Lehmann, and B. H. Pate, Molecular structure and chirality detection by Fourier transform microwave spectroscopy, J. Phys. Chem. Lett. **6**, 196 (2015).

[14] V. A. Shubert, D. Schmitz, C. Pérez, C. Medcraft, A. Krin, S. R. Domingos, D. Patterson, and M. Schnell, Chiral analysis using broadband rotational spectroscopy, J. Phys. Chem. Lett. **7**, 341 (2015).

[15] K. K. Lehmann, Proposal for chiral detection by the ac Stark-effect, arXiv:1501.05282; Stark field modulated microwave detection of molecular chirality, arXiv:1501.07874.

[16] K. K. Lehmann, Influence of spatial degeneracy on rotational spectroscopy: Three-wave mixing and enantiomeric state separation of chiral molecules, J. Chem. Phys. **149**, 094201 (2018).

[17] C. Ye, Q. Zhang, Y.-Y. Chen, and Y. Li, Determination of enantiomeric excess with chirality-dependent ac Stark effects in cyclic three-level models, Phys. Rev. A **100**, 033411 (2019).

[18] X.-W. Xu, C. Ye, Y. Li, and A.-X. Chen, Enantiomeric-excess determination based on nonreciprocal-transition-induced spectral-line elimination, Phys. Rev. A **102**, 033727 (2020).

[19] Y.-Y. Chen, C. Ye. Q. Zhang, and Y. Li, Enantio-discrimination via light deflection effect, J. Chem. Phys. **152**, 204305 (2020).

[20] C. Ye, Y. Sun, and X. Zhang, Entanglement-assisted quantum chiral spectroscopy, J. Phys. Chem. Lett. **12**, 8591 (2021).

[21] Y.-X. Liu, J. Q. You, L. F. Wei, C. P. Sun, and F. Nori, Optical Selection Rules and Phase-Dependent Adiabatic State Control in a Superconducting Quantum Circuit, Phys. Rev. Lett. **95**, 087001 (2005).

[22] Y. Li, L. Zheng, Y.-X. Liu, and C. P. Sun, Correlated photons and collective excitations of a cyclic atomic ensemble, Phys. Rev. A **73**, 043805 (2006).

[23] E. Hirota, Triple resonance for a three-level system of a chiral molecule, Proc. Jpn. Acad., Ser. B **88**, 120 (2012).

[24] L. Zhou, L.-P. Yang, Y. Li, and C. P. Sun, Quantum Routing of Single Photons with a Cyclic Three-Level System, Phys. Rev. Lett. **111**, 103604 (2013).

[25] C. Ye, Q. Zhang, and Y. Li, Real single-loop cyclic three-level configuration of chiral molecules, Phys. Rev. A **98**, 063401 (2018).

[26] N. V. Vitanov and M. Drewsen, Highly Efficient Detection and Separation of Chiral Molecules through Shortcuts to Adiabaticity, Phys. Rev. Lett. **122**, 173202 (2019).

[27] J.-L. Wu, Y. Wang, J.-X. Han, C. Wang, S.-L. Su, Y. Xia, Y.-Y. Jiang, and J. Song, Two-Path Interference for Enantiomer-Selective State Transfer of Chiral Molecules, Phys. Rev. Appl. **13**, 044021 (2020).

[28] P. Král and M. Shapiro, Cyclic Population Transfer in Quantum Systems with Broken Symmetry, Phys. Rev. Lett. **87**, 183002 (2001).

[29] Y. Li and C. Bruder, Dynamic method to distinguish between left- and right-handed chiral molecules, Phys. Rev. A **77**, 015403 (2008).

[30] W. Z. Jia and L. F. Wei, Distinguishing left- and right-handed molecules using two-step coherent pulses, J. Phys. B: At., Mol. Opt. Phys. **43**, 185402 (2010).

[31] S. Eibenberger, J. M. Doyle, and D. Patterson, Enantiomer-Specific State Transfer of Chiral Molecules, Phys. Rev. Lett. **118**, 123002 (2017).

[32] C. Pérez, A. L. Steber, S. R. Domingos, A. Krin, D. Schmitz, and M. Schnell, Coherent enantiomer-selective population enrichment using tailored microwave fields, Angew. Chem., Int. Ed. **56**, 12512 (2017).

[33] C. Ye, Q. Zhang, Y.-Y. Chen, and Y. Li, Effective two-level models for highly efficient inner-state enantioseparation based on cyclic three-level systems of chiral molecules, Phys. Rev. A **100**, 043403 (2019).

[34] M. Leibscher, T. F. Giesen, and C. P. Koch, Principles of enantio-selective excitation in three-wave mixing spectroscopy of chiral molecules, J. Chem. Phys. **151**, 014302 (2019).

[35] Q. Zhang, Y.-Y. Chen, C. Ye, and Y. Li, Evading thermal population influence on enantiomeric-specific state transfer based on a cyclic three-level system via ro-vibrational transitions, J. Phys. B: At., Mol. Opt. Phys. **53**, 235103 (2020).

[36] B. T. Torosov, M. Drewsen, and N. V. Vitanov, Chiral resolution by composite Raman pulses, Phys. Rev. Research **2**, 043235 (2020).

[37] Y. Li, C. Bruder, and C. P. Sun, Generalized Stern-Gerlach Effect for Chiral Molecules, Phys. Rev. Lett. **99**, 130403 (2007).

[38] X. Li and M. Shapiro, Theory of the optical spatial separation of racemic mixtures of chiral molecules, J. Chem. Phys. **132**, 194315 (2010).

[39] A. Jacob and K. Hornberger, Effect of molecular rotation on enantioseparation, J. Chem. Phys. **137**, 044313 (2012).

[40] N. Kravets, A. Aleksanyan, and E. Brasselet, Chiral Optical Stern-Gerlach Newtonian Experiment, Phys. Rev. Lett. **122**, 024301 (2019).

[41] Y. Shi, T. Zhu, T. Zhang, A. Mazzulla, D. P. Tsai, W. Ding, A. Q. Liu, G. Cipparrone, J. J. Sáenz, and C.-W. Qiu, Chirality-assisted lateral momentum transfer for bidirectional enantioselective separation, Light: Sci. Appl. **9**, 62 (2020).

[42] B. Liu, C. Ye, C. P. Sun, and Y. Li, Spatial enantioseparation of gas chiral molecules, Phys. Rev. A **104**, 013113 (2021).

[43] R. Bennett, D. Steinbrecht, Y. Gorbachev, and S. Y. Buhmann, Symmetry Breaking in a Condensate of Light and its Use as a Quantum Sensor, Phys. Rev. Appl. **13**, 044031 (2020).

[44] X. Zhong, T. Chervy, S. Wang, J. George, A. Thomas, J. A. Hutchison, E. Devaux, C. Genet, and T. W. Ebbesen, Non-radiative energy transfer mediated by hybrid light-matter states, Angew. Chem., Int. Ed. **55**, 6202 (2016).

[45] R. Sáez-Blázquez, J. Feist, A. I. Fernández-Domínguez, and F. J. García-Vidal, Organic polaritons enable local vibrations to

drive long-range energy transfer, Phys. Rev. B **97**, 241407(R) (2018).
[46] A. D. Dunkelberger, B. T. Spann, K. P. Fears, B. S. Simpkins, and J. C. Owrutsky, Modified relaxation dynamics and coherent energy exchange in coupled vibration-cavity polaritons, Nat. Commun. **7**, 13504 (2016).
[47] F. Herrera and F. C. Spano, Dark Vibronic Polaritons and the Spectroscopy of Organic Microcavities, Phys. Rev. Lett. **118**, 223601 (2017).
[48] T. Neuman and J. Aizpurua, Origin of the asymmetric light emission from molecular exciton-polaritons, Optica **5**, 1247 (2018).
[49] Z. Zhang, K. Wang, Z. Yi, M. S. Zubairy, M. O. Scully, and S. Mukamel, Polariton-assisted cooperativity of molecules in microcavities monitored by two-dimensional infrared spectroscopy, J. Phys. Chem. Lett. **10**, 4448 (2019).
[50] F. Herrera and F. C. Spano, Cavity-Controlled Chemistry in Molecular Ensembles, Phys. Rev. Lett. **116**, 238301 (2016).
[51] J. A. Campos, R. F. Ribeiro, and J. Yuen-Zhou, Resonant catalysis of thermally activated chemical reactions with vibrational polaritons, Nat. Commun. **10**, 4685 (2019).
[52] J. Lather, P. Bhatt, A. Thomas, T. W. Ebbesen, and J. George, Cavity catalysis by cooperative vibrational strong coupling of reactant and solvent molecules, Angew. Chem., Int. Ed. **58**, 10635 (2019).
[53] Y.-H. Kang, Z.-C. Shi, J. Song, and Y. Xia, Effective discrimination of chiral molecules in a cavity, Opt. Lett. **45**, 4952 (2020).
[54] Y.-Y. Chen, C. Ye, and Y. Li, Enantio-detection via cavity-assisted three-photon processes, Opt. Express **29**, 36132 (2021).
[55] A. Salam and W. J. Meath, On the control of excited state relative populations of enantiomers using circularly polarized pulses of varying durations, J. Phys. Chem. **106**, 7865 (1997).
[56] A. Salam and W. J. Meath, On enantiomeric excesses obtained from racemic mixtures by using circularly polarized pulsed lasers of varying durations, Chem. Phys. **228**, 115 (1998).
[57] J. Shao and P. Hänggi, Control of molecular chirality, J. Phys. Chem. **107**, 9935 (1997).
[58] M. Shapiro, E. Frishman, and P. Brumer, Coherently Controlled Asymmetric Synthesis with Achiral Light, Phys. Rev. Lett. **84**, 1669 (2000).
[59] D. Gerbasi, M. Shapiro, and P. Brumer, Theory of enantiomeric control in dimethylallene using achiral light, J. Chem. Phys. **115**, 5349 (2001).
[60] P. Brumer, E. Frishman, and M. Shapiro, Principles of electric-dipole-allowed optical control of molecular chirality, Phys. Rev. A **65**, 015401 (2001).
[61] K. Hoki, L. González, and Y. Fujimura, Quantum control of molecular handedness in a randomly oriented racemic mixture using three polarization components of electric fields, J. Phys. Chem. **116**, 8799 (2002).
[62] P. Král, I. Thanopulos, M. Shapiro, and D. Cohen, Two-Step Enantio-Selective Optical Switch, Phys. Rev. Lett. **90**, 033001 (2003).
[63] C. Ye, Q. Zhang, Y.-Y. Chen, and Y. Li, Fast enantioconversion of chiral mixtures based on a four-level double-Δ model, Phys. Rev. Research **2**, 033064 (2020).
[64] C. Ye, Q. Zhang, Y.-Y. Chen, and Y. Li, Improved laser-distillation method for complete enantio-conversion of chiral mixtures, J. Phys. B: At., Mol. Opt. Phys. **54**, 145102 (2021).
[65] C. Ye, B. Liu, Y.-Y. Chen, and Y. Li, Enantio-conversion of chiral mixtures via optical pumping, Phys. Rev. A **103**, 022830 (2021).
[66] H. Wang, D. J. Goorskey, and M. Xiao, Bistability and instability of three-level atoms inside an optical cavity, Phys. Rev. A **65**, 011801(R) (2001).
[67] H. Wu, J. Gea-Banacloche, and M. Xiao, Observation of Intracavity Electromagnetically Induced Transparency and Polariton Resonances in a Doppler-Broadened Medium, Phys. Rev. Lett. **100**, 173602 (2008).
[68] R. Culver, A. Lampis, B. Megyeri, K. Pahwa, L. Mudarikwa, M. Holynski, P. W. Courteille, and J. Goldwin, Collective strong coupling of cold potassium atoms in a ring cavity, New J. Phys. **18**, 113043 (2016).
[69] T. Holstein and H. Primakoff, Field dependence of the intrinsic domain magnetization of a ferromagnet, Phys. Rev. **58**, 1098 (1940).
[70] A. Klein and E. R. Marshalek, Boson realizations of Lie algebras with applications to nuclear physics, Rev. Mod. Phys. **63**, 375 (1991).
[71] C. P. Sun, Y. Li, and X. F. Liu, Quasi-Spin-Wave Quantum Memories with a Dynamical Symmetry, Phys. Rev. Lett. **91**, 147903 (2003).
[72] C. Emary and T. Brandes, Quantum Chaos Triggered by Precursors of a Quantum Phase Transition: The Dicke Model, Phys. Rev. Lett. **90**, 044101 (2003).
[73] G. R. Jin, P. Zhang, Y.-X. Liu, and C. P. Sun, Superradiance of low-density Frenkel excitons in a crystal slab of three-level atoms: The quantum interference effect, Phys. Rev. B **68**, 134301 (2003).
[74] Z. Kurucz and K. Mølmer, Multilevel Holstein-Primakoff approximation and its application to atomic spin squeezing and ensemble quantum memories, Phys. Rev. A **81**, 032314 (2010).
[75] A. Baksic, P. Nataf, and C. Ciuti, Superradiant phase transitions with three-level systems, Phys. Rev. A **87**, 023813 (2013).
[76] C. R. Ayrea and R. J. Madix, The adsorption and reaction of 1,2-propanediol on Ag(110) under oxygen lean conditions, Surf. Sci. **303**, 279 (1994).
[77] R. N. Zare, *Angular Momentum* (Wiley, New York, 1988).
[78] B. E. Arenas, S. Gruet, A. L. Steber, and M. Schnell, A global study of the conformers of 1,2-propanediol and new vibrationally excited states, J. Mol. Spec. **337**, 9 (2017).
[79] C. Gardiner and P. Joller, *Quantum Noise* (Springer, Berlin, 2004).
[80] D. F. Walls and G. J. Milburn, *Quantum Optics*, 2nd ed. (Springer, Berlin, 2008).
[81] G. S. Agarwal, *Quantum Optics* (Cambridge University Press, Cambridge, UK, 2013).
[82] T. Kampschulte and J. H. Denschlag, Cavity-controlled formation of ultracold molecules, New J. Phys. **20**, 123015 (2018).
[83] N. Hoghooghi, R. J. Wright, A. S. Makowiecki, W. C. Swann, E. M. Waxman, I. Coddington, and G. B. Rieker, Broadband coherent cavity-enhanced dual-comb spectroscopy, Optica **6**, 28 (2019).
[84] M. Tavis and F. W. Cummings, Exact solution for an N-molecule–radiation-field hamiltonian, Phys. Rev. **170**, 379 (1968).